JOURNAL OF MATERIALS SCIENCE 19 (1984) 2098–2110

# An electron microscopy and X-ray diffraction study of the microstructures of melt-drawn polyethylene films

D. C. YANG,* EDWIN L. THOMAS
*Polymer Science and Engineering Department, University of Massachusetts, Amherst, Massachusetts 01003, USA*

Electron microscopy and X-ray diffraction have been used to study microstructures of melt-drawn polyethylene films. During the drawing process, uniplanar structures are formed which consist of crystals with their *b* and *c* axes in the film plane. On annealing the films, the crystal size and orientation increase. Quantitative measures of the crystal thickness, lateral crystallite size and long period were obtained from bright-field and dark-field electron micrographs as well as from wide and small angle X-ray diffraction of stacked layers of the films.

## 1. Introduction

In recent years considerable attention has been focused on the morphology and the crystallization mechanisms of fibres prepared by strain induced crystallization [1–3]. Theoretical explanations are based on longitudinal flow gradients developed in solutions or melts during various processes [4–6]. In order to obtain polymeric materials with high orientation, an effective approach is to increase the longitudinal flow gradient. In industry a high longitudinal flow gradient is achieved by employing spinning velocities on the order of $1 \times 10^4$ cm sec$^{-1}$ [7]. For laboratory investigations, the method developed by Petermann [8, 9] is convenient. Here the high longitudinal flow gradient is produced using relatively low take-up speeds (approximately 1 cm sec$^{-1}$) by developing the flow over an extremely small region (approximately 1 $\mu$m). The crystallization mechanisms and morphology of several semi-crystalline polymers and their blends have been extensively investigated by Petermann and co-workers using the above method [3, 8–14].

The purpose of this paper is to study the detailed morphology of melt-drawn polyethylene films. We report various quantitative measures of the as-drawn and annealed microstructure by means of electron microscopy, electron diffraction and small and wide angle X-ray scattering.

## 2. Experimental methods

The high density polyethylene utilized in this work is Marlex 6003 (mol. wt $= 2 \times 10^5$). Highly oriented crystalline films of polyethylene were prepared according to the method by Petermann and Gohil [8] under very high longitudinal flow gradients of the order of $10^4$ sec$^{-1}$. A polyethylene solution (concentration of 0.5 weight per cent) in xylene was uniformly spread on a preheated (120 to 125° C) glass plate and the solvent allowed to evaporate at the preparation temperature. A thin supercooled polyethylene film was then quickly drawn off vertically from the glass surface (see Fig. 1). The take-up speed was 4 cm sec$^{-1}$. This procedure yields films of 50 to 100 nm thickness, which were directly used for transmission electron microscopy (TEM) investigations. By continuously winding the film on a roller, thicker samples of about 2000 layers could be obtained, which were then subsequently stacked and used for the small angle X-ray scattering (SAXS) and wide angle X-ray scattering (WAXS) measure-

*Permanent address: Polymer Structure Laboratory, Changchun Institute of Applied Chemistry, People's Republic of China.


0022–2461/84 $03.00 + .12 

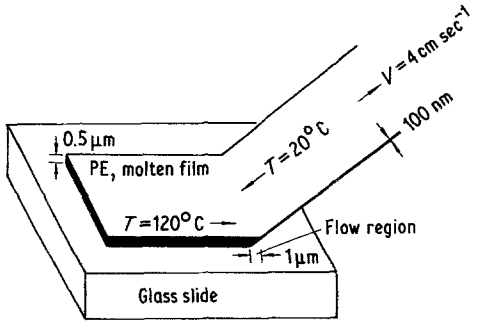


*Figure 1* Schematic diagram of the Petermann [8] method of preparing oriented films.

ments. Final sample thickness for X-ray work was about 0.5 to 1 mm. Annealing of the individual thin films was carried out on the surface of glycerol at 128° C for 2 h, or for the stacked films in a vacuum oven at 128° C for 2 h.

Transmission electron microscopy was performed using a JEOL 100 CX microscope operated at 100 kV. In order to stabilize the films against dimensional changes from the electron beam, a thin layer of carbon was evaporated onto the surface of the films. Phase contrast and ghost image electron micrographs were obtained by defocus of the objective lens [12, 15, 16]. In order to minimize radiation damage, the focusing was carried out on an area, then the film was translated to an adjacent undamaged area and the image recorded on Kodak S0-163 film using approximately 60% of the crystal lifetime. Microdensitometry scans were performed on an Optronics P2000 photoscan.

A Perkin Elmer DSC II was used to characterize the melting behaviour of the samples. The temperature scale and energy input of the DSC were calibrated using the melting transition and heat of fusion of an indium standard. The heating rate was 20° C $min^{-1}$ with sample size of about 5 mg.

SAXS experiments were carried out on the ORNL 10 metre camera [17] using Cu$K\alpha$ radiation with a sample to detector distance of 5 m. Data from the two-dimensional position sensitive detector was corrected for detector sensitivity, parasitic scattering (from the pinhole collimators) and detector electronic noise. The long period was measured from linearly averaged intensity slices parallel to the orientation direction. The typical measuring time was 1000 sec.

WAXS profiles of the (1 1 0) and (0 0 2) reflections were recorded using a Siemens D500 wide angle diffractometer employed in the symmetric transmission mode with nickel filtered Cu$K\alpha$ radiation. The beam divergence was minimized for line broadening measurements with 0.1° incident beam slits and a 0.018° receiving slit so that a 2.0 mm thick hexamethylene tetramine standard had integral breadths of 0.03° and 0.1° for the reflections at 17.89° and 73.76° $2\theta$, respectively. The Rachinger correction [18] was applied to remove the Cu$K\alpha_{II}$ peak from the profiles. The correction of the observed integral breadths for instrumental broadening was assumed to be of the form:

$$\Delta\beta_{obs} = \Delta\beta_L + \Delta\beta_{instr.} \quad (1)$$

where $\Delta\beta_{obs}$ indicates the integral breadth, $\Delta\beta_L$ is the broadening from the sample, and $\Delta\beta_{instr.}$ is the instrumental broadening. The Scherrer equation was used to calculate the mean size of the crystals:

$$L_{hkl} = \frac{K\lambda}{\Delta\beta_{hkl}\cos\theta_{hkl}}. \quad (2)$$

$K$ was taken as 1.0 for the (1 1 0) and the (0 0 2) reflections [19].

## 3. Results and discussion

During the preparation process of melt-drawn polyethylene films, the crystallization of the polyethylene melt is induced by a high longitudinal flow gradient. The flow region can be measured by allowing the undrawn portion of the polyethylene melt to cool and crystallize and then examining a portion of this film containing adjacent drawn and undrawn regions [8]. For our conditions, the flow region is found to be about one micrometre. From the measured values of the initial (0.5 $\mu$m) and final (0.1 $\mu$m) film thickness, the film is deformed by a factor of five during the melt drawing process.

Fig. 2 shows bright-field defocus phase contrast electron micrographs of as-drawn and annealed (for 2 h at 128° C) polyethylene films before and after radiation damage. The arrows indicate the drawing direction. The electron diffraction pattern (see insert), indicates the films consist of crystallites with the molecular axis ($c$ axis) well-aligned with the direction of drawing. In the underfocused bright-field images, the lower mean inner potential of the non-crystalline interlamellar regions (6.32 V) with respect to that of the crystalline lamellae regions (7.35 V) causes the interlamellar zones to appear as bright lines [12, 13]. The grey areas between the bright lines are the crystalline lamellae

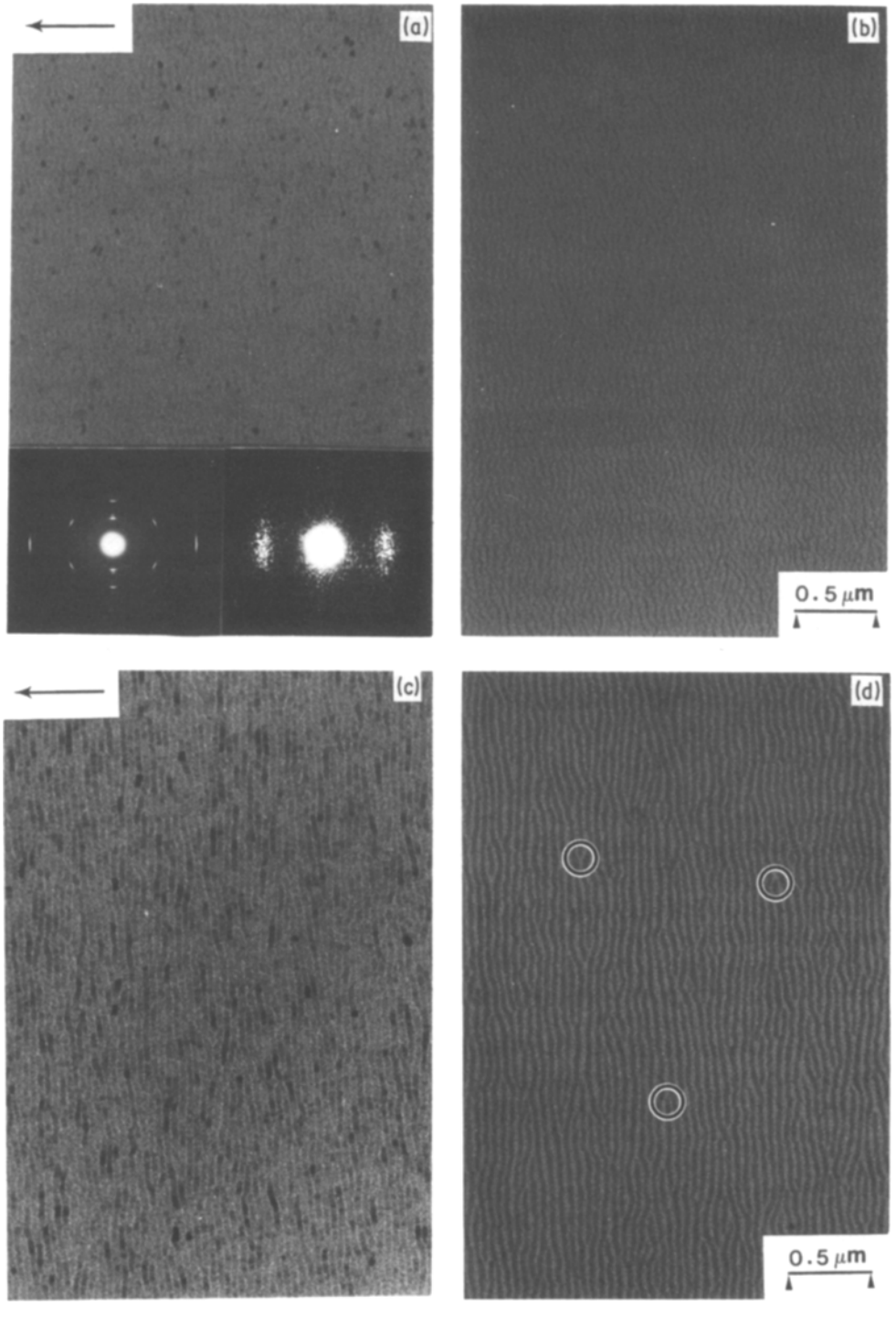


*Figure 2* Bright-field phase contrast (objective lens underfocus − 1.7 μm) electron micrographs and electron and optical diffraction patterns (inset) of PE films. The arrows show the drawing direction. (a) As-drawn film; (b) radiation damaged as-drawn film; (c) annealed film; (d) radiation damaged annealed film.

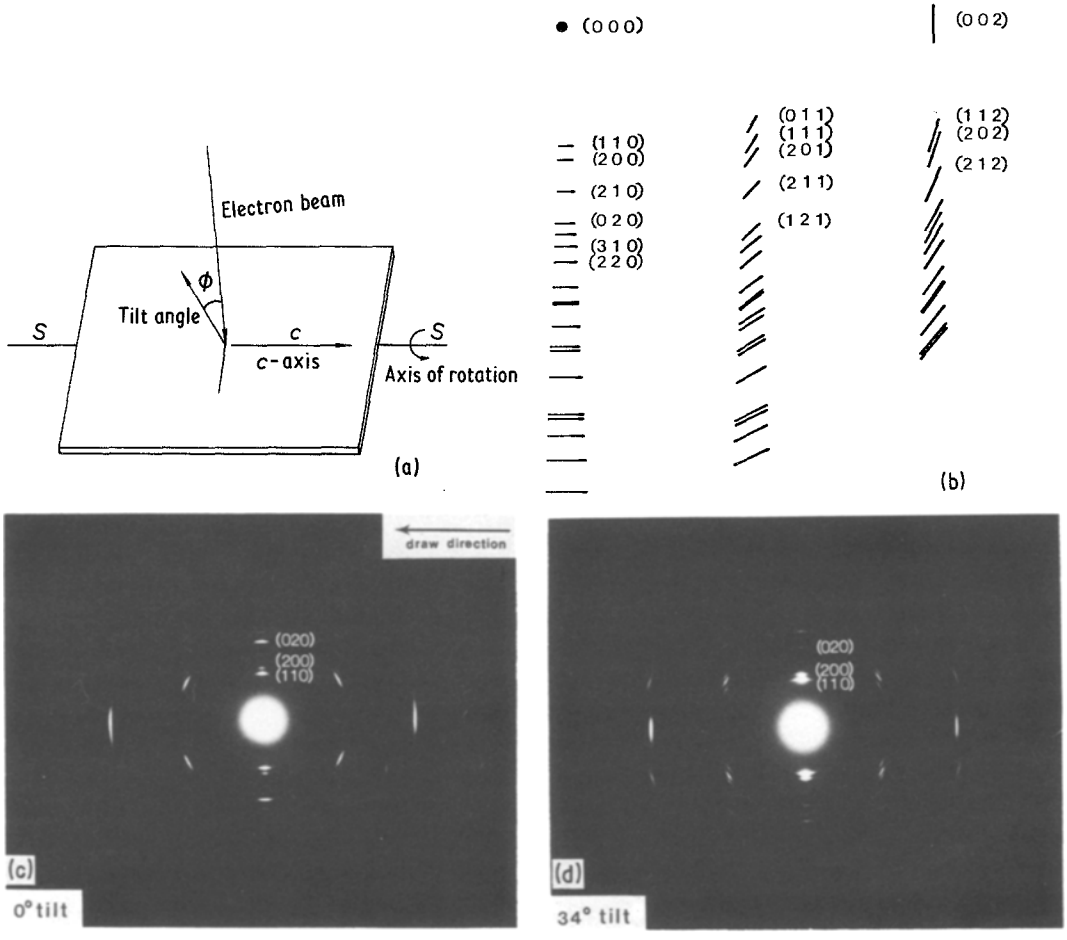


*Figure 3* Electron diffraction study of as-drawn and annealed polyethylene films. (a) Diagram showing the geometry of film tilt with respect to the electron beam direction. (b) Indexed electron diffraction pattern of PE with fibre symmetry. (c) As-drawn, tilt angle $\phi = 0°$. (d) As-drawn, tilt angle $\phi = 34°$. (e) Annealed, tilt angle $\phi = 0°$. (f) Annealed, tilt angle $\phi = 34°$. (g) Equatorial microdensitometer traces of as-drawn film. (h) Equatorial microdensitometer traces of annealed film.

(see Fig. 2c). The various dark patches represent lamellar regions which are Bragg oriented with respect to the incident electron beam.

Figs. 2b and d are bright-field defocus electron micrographs of a radiation damaged area of the as-drawn and annealed films. For such radiation damaged areas, the diffraction effects disappear and the dimensions of the microstructure are altered. It is interesting to note that beam damage results in an approximate 24% contraction of the lamellar thickness, while because of the accompanying expansion of the material in the interlamellar regions, the long period is nearly unchanged. Although radiation damage causes a substantial change in the contrast of the image. the resulting morphology still permits ready determination of the length of the lamellae along the direction perpendicular to the drawing and the orientation of the surface normal of the lamellae with respect to the draw direction. The as-drawn film consists of rather "wavy" lamellae, with lengths ranging from 0.2 $\mu$m up to 0.5 $\mu$m. The lamellae in the annealed film are much straighter and longer, ranging upwards of 10 $\mu$m in length with only occasional short (0.1 $\mu$m) lamellae. The angular range of the surface normals in both types of film has values up to $\pm 30°$, particularly in regions where the lamellae branch or end (see circled regions in Fig. 2d).

Electron diffraction patterns of as-drawn and annealed polyethylene films also indicate the improvement of overall crystal orientation from the decrease in the arcing of the reflections (compare Figs. 3c and e). The intensities of the dif-

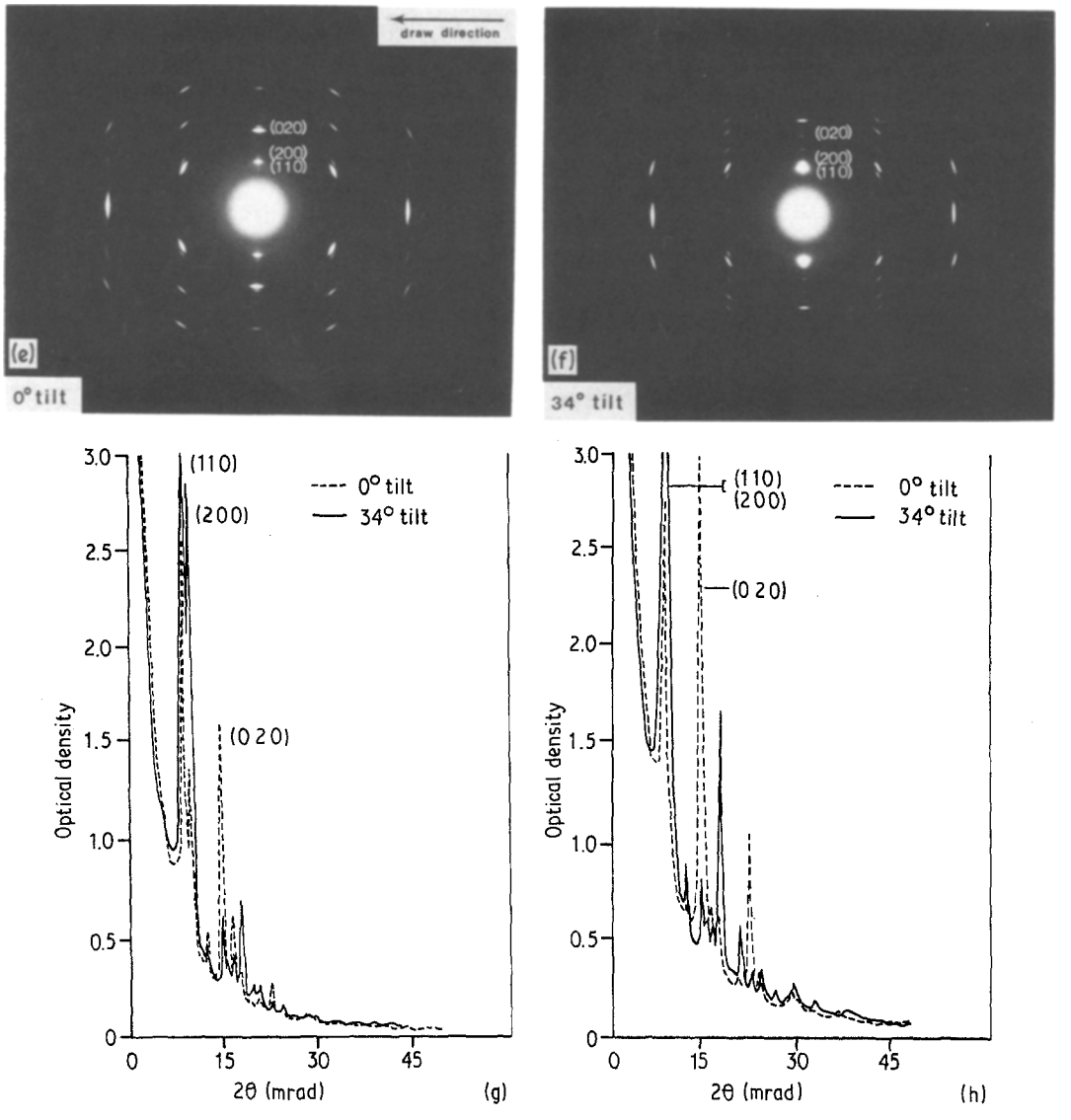


*Figure 3* Continued.

fraction spots depend on the rotation angle ($\phi$) about the draw direction (see Fig. 3a). At an angle of approximately $\phi = \pm 34^\circ$ (Fig. 3d) the intensity of the (1 1 0) reflection is significantly increased whereas the (0 2 0) reflection, is considerably decreased (for a schematic showing pattern indexing see Fig. 3b). This indicates the presence of an asymmetrical fibre structure in these thin films. This is unlike the melt-drawn PE films produced by Petermann [14] which showed true fibre symmetry. This earlier work employed lower molecular weight PE with molten orthophosphoric acid as the substrate, which resulted in a much more gradual draw zone (1 cm compared to 1 $\mu$m on glass).

The electron diffraction patterns of films annealed for 2 h at 120° C, 124° C, 128° C or 132° C all show this same type of behaviour with specimen tilt. Figs. 3e and f, as an example, indicate the change of the electron diffraction pattern with rotation for a specimen annealed at 128° C for 2 h. Note the large variation of the (0 2 0) intensity with tilt. The changes of the intensities of the electron diffraction patterns with tilt angle can be quantified by microdensitometry. Figs. 3g and h display microdensitometer traces along the zero layer line for the as-drawn and annealed film respectively. Numerical data of the intensity changes with tilt angle for selected reflections are listed in Table I. Structure factors

TABLE I Calculated structure factors and experimentally observed intensity changes with tilt angle for selected polyethylene reflections.

| $hkl$ | $2\theta$ (mrad) | $d_{hkl}$ (nm) | Single crystal | | Symmetrical fibre | Experimental values (optical densities) | | | | | | | |
|---|---|---|---|---|---|---|---|---|---|---|---|---|---|
| | | | $F^2$ (nm) | $F^2/F^2_{110}$ | $F^2/F^2_{110}$ | As-drawn film | | | | Annealed film | | | |
| | | | | | | 0° | | 34° | | 0° | | 34° | |
| | | | | | | $I_{hkl}$ | $I_{hkl}/I_{110}$ | $I_{hkl}$ | $I_{hkl}/I_{110}$ | $I_{hkl}$ | $I_{hkl}/I_{110}$ | $I_{hkl}$ | $I_{hkl}/I_{110}$ |
| 110 | 9 | 0.410 | 0.9197 | 1.00 | 1.00 | 2.04 | 1.00 | 2.40 | 1.00 | 1.89 | 1.00 | 2.79 | 1.00 |
| 200 | 10 | 0.369 | 0.6856 | 0.74 | 0.60 | 0.87 | 0.43 | 2.35 | 0.98 | 0.15 | 0.08 | 1.56 | 0.56 |
| 020 | 15 | 0.246 | 0.2788 | 0.30 | 0.11 | 1.54 | 0.75 | 0.44 | 0.18 | 2.54 | 1.34 | 0.45 | 0.16 |
| 002 | 29 | 0.127 | 0.1797 | 0.19 | 0.02 | 2.17 | 1.06 | 2.11 | 0.88 | 2.83 | 1.50 | 2.45 | 0.88 |
| 011 | 16 | 0.225 | 0.1497 | 0.16 | 0.05 | 1.55 | 0.76 | 0.62 | 0.26 | 2.59 | 1.37 | 0.77 | 0.28 |
| 310 | 17 | 0.220 | 0.1011 | 0.11 | 0.03 | 0.43 | 0.22 | 0.22 | 0.09 | 0.30 | 0.16 | 0.27 | 0.10 |
| 112 | 31 | 0.121 | 0.0816 | 0.09 | 0.01 | 0.33 | 0.16 | 0.77 | 0.32 | 0.75 | 0.39 | 1.62 | 0.58 |
| 111 | 17 | 0.216 | 0.0612 | 0.06 | 0.02 | 0.40 | 0.19 | 1.15 | 0.48 | 0.92 | 0.48 | 1.76 | 0.63 |
| 220 | 18 | 0.205 | 0.0395 | 0.04 | 0.01 | 0.17 | 0.08 | 0.59 | 0.25 | 0.32 | 0.17 | 1.42 | 0.51 |

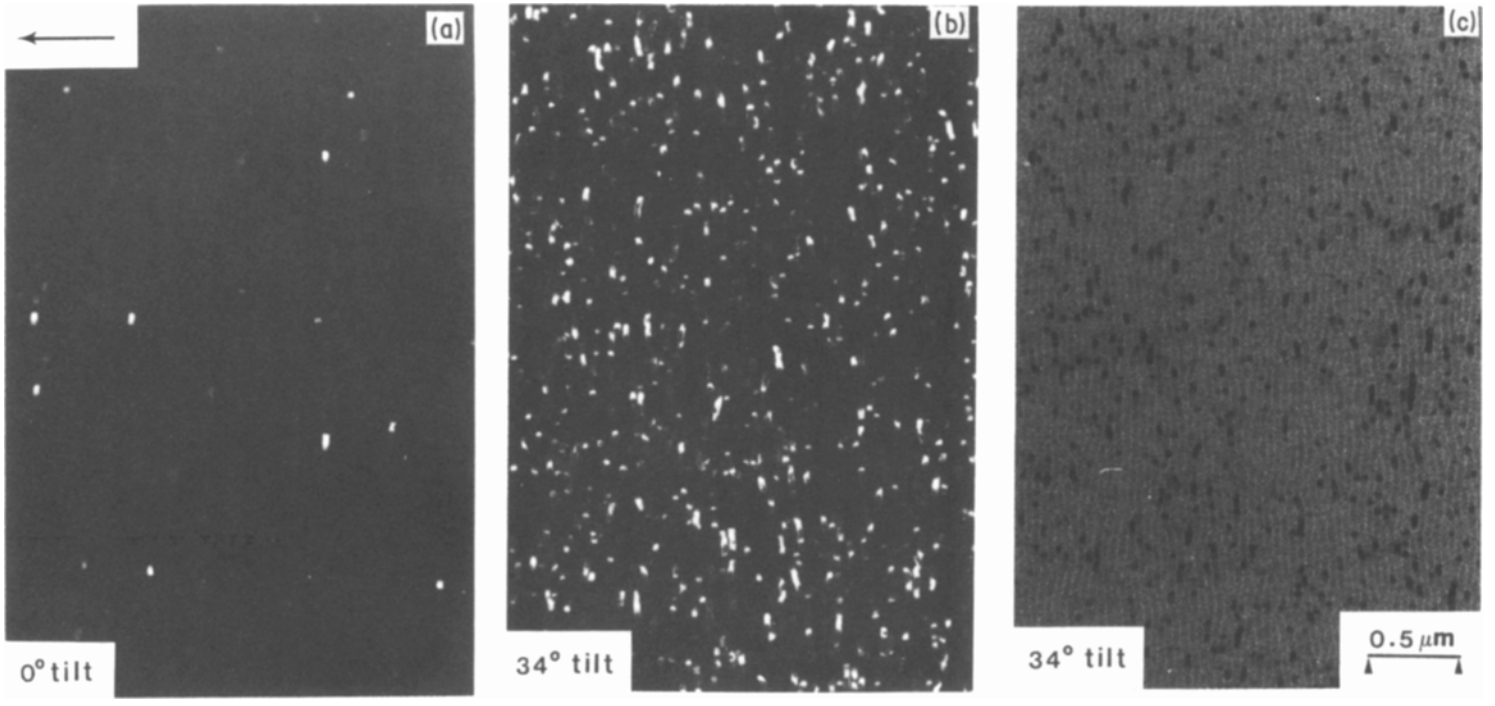


*Figure 4* Dark-field electron micrographs (a, b) of the (1 1 0) reflection and corresponding bright-field phase contrast electron micrograph (c) for melt-drawn polyethylene films annealed for 2 h at 128° C.

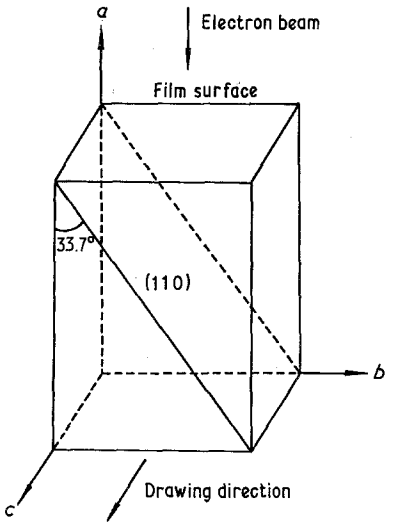


*Figure 5* Diagram showing the orientation of the crystals in melt-drawn polyethylene film with respect to the electron beam of the microscope.

for polyethylene single crystal and symmetrical fibre patterns are included for comparison.

Figs. 4a and b are (1 1 0) dark-field electron micrographs of an annealed (2 h at 128° C) film for tilt angles of 0° and 34°, respectively. The number of the bright regions [due to Bragg diffraction from the (1 1 0) planes] becomes maximum at tilt angles of ± 34°, consistent with the results of electron diffraction patterns. Fig. 4c shows the corresponding ($\phi = +34°$) bright-field micrograph exhibiting both phase and diffraction contrast. It is especially noticeable by comparing Fig. 4c with Fig. 2c that the number of very dark patches [which represent the strongly diffracting (1 1 0) regions] attains a maximum while the number of regions of intermediate darkness [from other less intense ($h k l$) reflections] decreases significantly. The texture of the film is thus approximately a (2 0 0) surface (see Fig. 5). The films studied by Petermann which initially displayed fibre symmetry underwent surface controlled recrystallization to a {1 1 0} surface plane upon annealing [14].

A bright field "ghost" image is shown in Fig. 6a. White diffraction images occur when the objective lens is defocused and no limiting objective aperture is used [15, 16]. From knowledge of the direction and magnitude of the image shift, from the relative intensity of ghost images and by comparison to corresponding single beam dark-field images, it is found that only the (1 1 0) and (2 0 0) reflections produce visible ghost images. An interesting feature is that sometimes these ($h k 0$) ghost images do not shift parallel to the plane of the lamellae (see regions A and B in Fig. 6a). Such non-parallel shifts indicate that the diffracting planes are inclined to the lamellar surface (see Fig. 6b). Since the chain axis is parallel to the ($h k 0$) planes, the chains in these regions are therefore oblique to the lamellar surface. Fig. 6c is a histogram of the distribution of the various inclination angles obtained from analysis of ghost images. From a measurement of about 100 ghost images, the range of chain inclination angle in the annealed films is from 0° up to about 24°. The average value is about 6°. While non-parallel ghost image shifts sometimes occur in regions of deviation of the lamellar normal from the draw direction, non-parallel shifts also occur in regions where the lamellae run normal to the direction of draw.

Electron micrographs have previously been used to obtain quantitative information about lamellar morphology [20–23]. The present films are particularly suitable for this and moreover, with the availability of sufficient sample, can provide a direct test of the correspondence between EM and WAXS and SAXS measures of the microstructure. Numerical data from electron micrographs were obtained by measuring the lamellar thickness and corresponding long period as well as the lateral crystallite size (from diffracting regions) and are presented in the form of histograms. Figs. 7a and b show the histograms of the lamellar thickness and long period derived from BF electron micrographs for the as-drawn and annealed specimens. The average thickness of the lamellae increases about 10 nm as a result of annealing, with only a slight increase of the long period. This trend is also observed in the average long period obtained from optical diffraction of the BF phase contrast electron micrograph negatives (see insert in Fig. 2a). The two-dimensional SAXS isointensity contour plots of the as-drawn and annealed films are shown in Fig. 8a. Both samples exhibit prominent two-point patterns. A weak second order peak is present in the annealed sample (see Fig. 8b). The strong equatorial scatter (along $S_2$) from long, thin voids in the as-drawn films is significantly reduced by annealing. The vaues of the long period obtained from the histograms, optical diffractometry and SAXS are all in reasonable agreement (see Table II). The linear degree of crystallinity, i.e. the ratio of the crystal thickness to the long

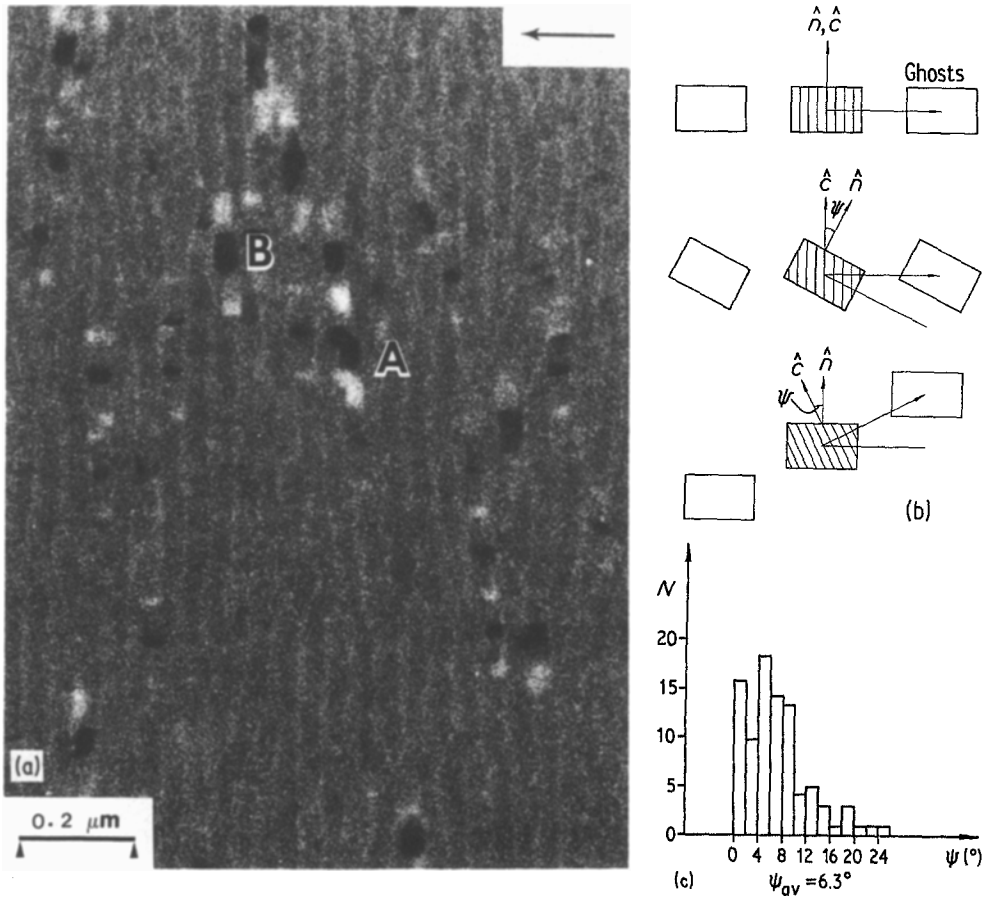


*Figure 6* (a) Bright-field "ghost" image of melt-drawn polyethylene film annealed for 2 h at 128° C. (b) Diagrams of chain inclination angle. (c) Histogram distribution of the tilt angles obtained from ghost images.

period, increases from about 0.55 to 0.76 with annealing, in rough agreement with the values of the crystallinity determined by DSC (0.67 and 0.82 respectively).

In addition to an increase in the crystal orientation, thickness and long period, annealing also results in a significant increase of the length of the lamellae and the lateral size of the crystals. The lateral size can be determined from the (1 1 0) WAXS peak width and the thickness from the peak width of the (0 0 2) reflection. The increase of the lateral width with annealing from 26.5 nm to 36.0 nm is larger than that of the thickness (from 31.7 nm to 36.3 nm) (see Table II). Dark-field electron micrographs prove this aspect directly. Small, nearly equiaxed crystallites with average dimensions of about 25 nm are visible in the (1 1 0) DF micrograph of the as-drawn film (Fig. 9a), whereas considerably longer and somewhat thicker crystallites appear in the annealed film (see Fig. 4b). The crystallite width distributions are shown in Fig. 10. The crystallite width distribution of the annealed specimen exhibits a significant tail of very long (0.1 μm) crystallites.

Dark-field micrographs were also carefully examined in order to identify any needle-like

TABLE II Microstructural features of polyethylene films.

| Samples | Lamellar thickness (nm) | | Long period (nm) | | | Crystallite width (nm) | |
|---|---|---|---|---|---|---|---|
| | TEM (BF) | WAXS (0 0 2) | TEM (BF) | Optical | SAXS | TEM (DF) | WAXS (1 1 0) |
| As-drawn | 27.8 | 31.7 | 45.2 | 42.9 | 44.1 | 24.0 | 26.5 |
| Annealed | 36.7 | 36.3 | 48.1 | 49.9 | 48.2 | 42.5 | 36.0 |

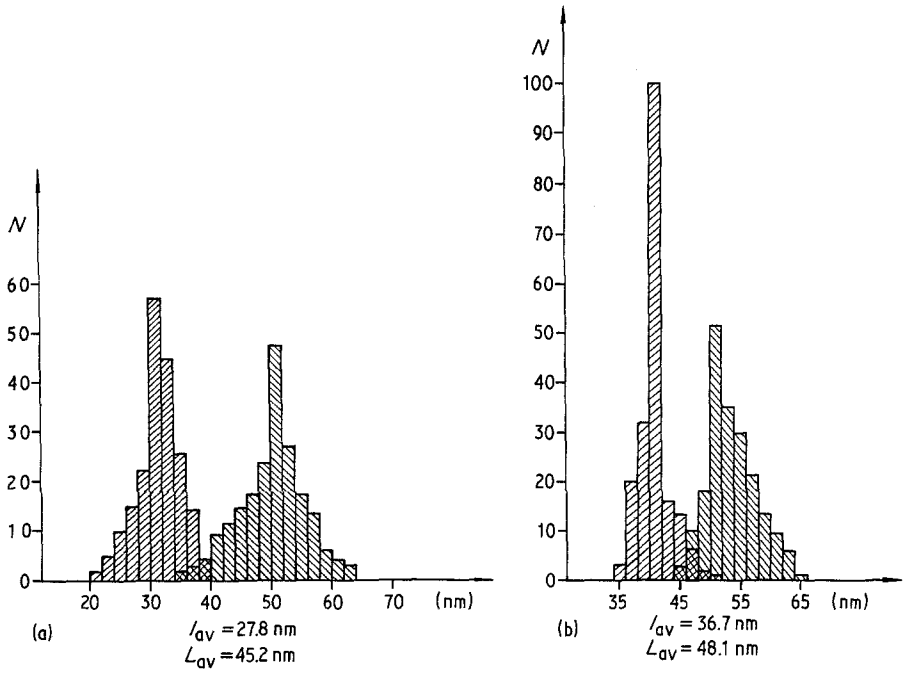


*Figure 7* Histograms showing long-period (\\\\) and crystal thickness (////) for (a) as-drawn film and (b) annealed film.

crystals present in the films. For the ~ 50 nm resolution attainable, no such structures were found, although the well-oriented crystallization of the lamellae must certainly stem from presence of some axial structures. Previous work by Petermann [8, 9] employing higher molecular weight PE and higher drawing temperatures showed approximately 10 nm diameter, micrometre long needle crystals using dark-field microscopy. Work in progress on the deformation of these PE films indicates that the interlamellar regions are essentially relaxed with relatively few needle-like crystals and/or taut tie molecules interconnecting the lamellae [24].

The crystallite size distribution determined by DF microscopy will be influenced by elastic bending of the crystals. DF will give a lower bound to the average crystal size since any distortion will serve to reduce the size of the coherently scattering region. The possible influence of elastic bending was explored by taking pairs of (1 1 0) DF micrographs with the specimen tilted between exposures by a small amount with respect to the incident beam direction. For accurate comparison of successive micrographs of the same area, the negatives were superposed, shifted slightly along the fibre axis and a composite micrograph printed (see Fig. 9b). For an approximate 1° tilt of the specimen between exposures, some long continuous but elastically bent crystalline regions should be tilted into the Bragg condition just adjacent to the previously diffracting region. For a sample consisting of small independent (undistorted) crystals, tilting will cause some crystals to completely disappear and other new crystals to appear. For the as-drawn film, this latter behaviour is observed, indicating the diffracting region size in the dark-field images is a correct measure of the actual crystalline size. The behaviour observed for the annealed films is consistent with the presence of a component of long, elastically bent crystals (see circled regions). Careful inspection shows that the types of regions which adjacently displace their diffracted intensity along their length have rather smooth variations of diffracted intensity at their ends, as opposed to the type of region for which the diffracted intensity abruptly drops to zero at the edges which uniformly extinguish upon tilt (see boxed regions). Such effects are consistent with elastically bent crystals in the former instance, and large angle grain boundaries between adjacent crystalline regions of a lamella in the latter. The lateral crystal width determined from line broadening analysis of the (1 1 0) reflection, which assumed the entire observed broadening was due to small crystal size effects alone, is thus in agreement with the dark-field results for the as-drawn film but not for the annealed film. In order properly to

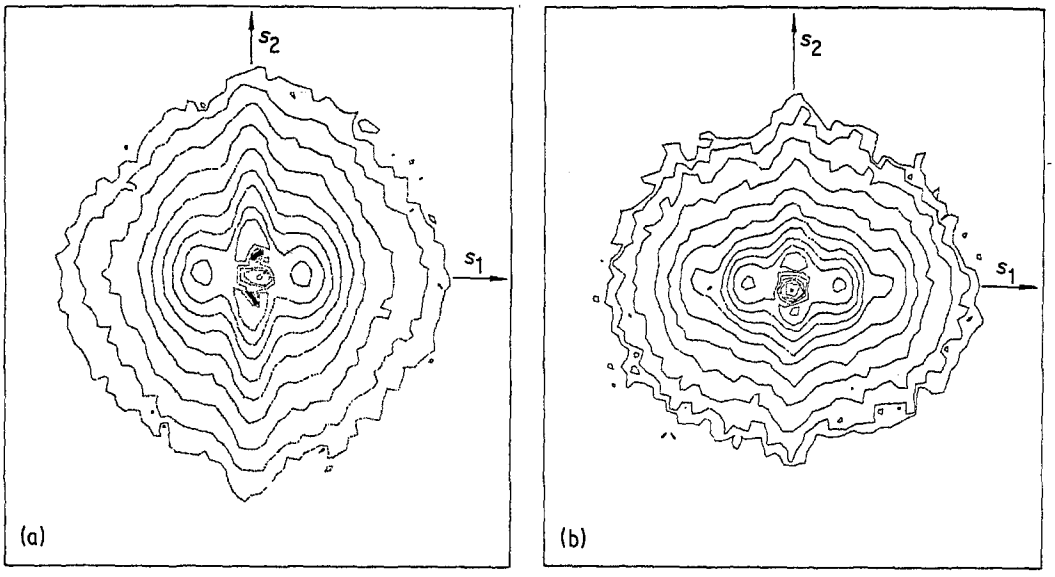


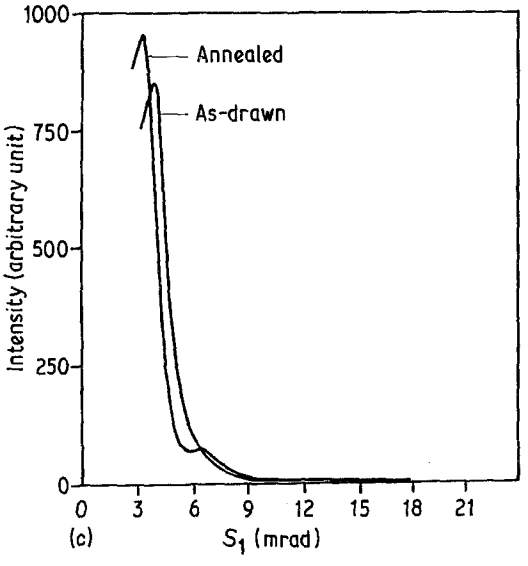


*Figure 8* (a) Two-dimensional isointensity SAXS contour plot for as-drawn and annealed PE films. (b) SAXS intensity traces along the $S_1$ (fibre) direction.

account for distortional broadening effects at least three orders of a reflection are required to differentiate size, strain and paracrystalline line broadening contributions [25]. Work along this direction is currently underway.

## 4. Summary

The melt drawing process results in crystallization into films containing a highly oriented lamellar structure. The lamellae in the as-drawn film are short and "wavy", that is, the normals to the lamellar surface vary about the draw direction by up to 30°. Electron diffraction shows the chain axis is better oriented than the lamellae. This itself necessitates the presence of a distribution of chain tilt angles, and bright-field ghost images of the annealed film show this effect directly. The as-drawn film does not possess fibre symmetry, but displays a (2 0 0) surface plane texture. The uniplanar texture is likely to be the result of the oriented nucleation in a thin film with the preference in PE for the *b* axis as the fast growth direction.

Annealing results in increased sample crystallinity, crystal thickness, (with only a slight increase in sample long period), significant lateral growth of the lamellae accompanied by lateral crystallite width growth, increased sample orientation without change in the (2 0 0) surface plane sample texture. The average thickness of the amorphous interlamellar region is reduced by almost one-half upon annealing. Good agreement is found between electron microscopy and small and wide X-ray scattering on all microstructural features except lateral crystallite width for the annealed films. DF microscopy shows the broad distribution of crystallite widths with a component of long ($\sim 0.1\,\mu$m) but easily elastically bent crystals and yields a significantly longer average crystalline width than that derived from WAXS line broadening.

## Acknowledgement

The financial support of the National Science Foundation, grant DMR 80-12724 (Polymers Program) is gratefully acknowledged. The authors

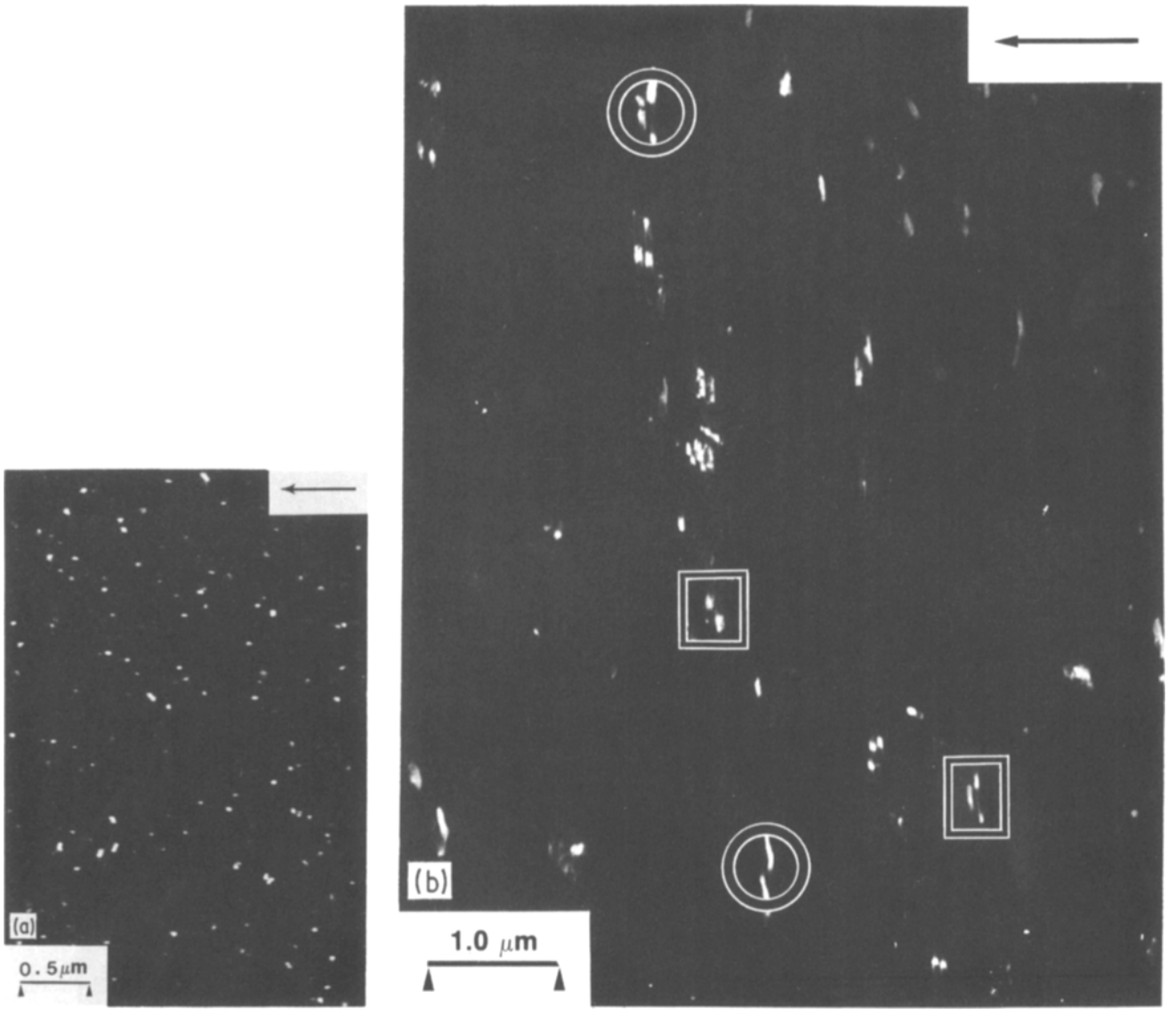


*Figure 9* Dark-field electron micrograph using the (110) reflection. (a) Image of as-drawn film. (b) Two superimposed images of the same area of an annealed film, but with a 1° tilt of the specimen between exposures and a small *c*-axis shift of the images with respect to one another.

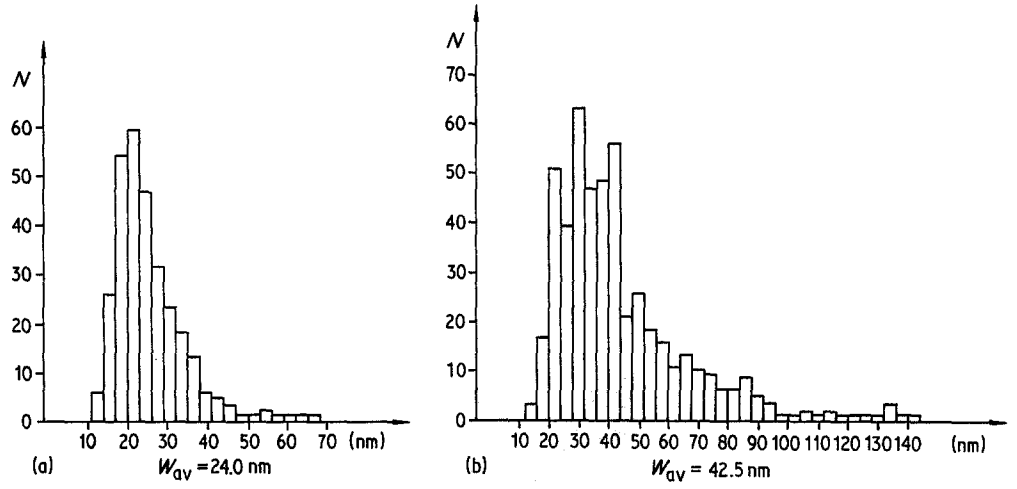


*Figure 10* Histograms showing the distributions of the lateral length of the crystals in polyethylene films. (a) From the (1 1 0) reflections for as-drawn film. (b) From the (1 1 0) reflections for annealed film.

also thank Professor J. Petermann for providing insight into the details of his sample preparation method; Mr D. Alward for the SAXS results; Mr X. Jin for DSC measurements; and Dr Wade Adams for the microdensitometry and helpful discussions.

## References

1. M. J. HILL and A. KELLER, *J. Macromol. Sci.* **B5** (1971) 591.
2. J. A. ODELL, D. T. GRUBB and A. KELLER, *Polymer* **19** (1978) 617.
3. J. PETERMANN, M. MILES and H. GLEITER, *J. Polymer Sci. Polymer Phys. Ed.* **17** (1979) 55.
4. F. C. FRANK, A. KELLER and M. R. MACKLEY, *Polymer* **12** (1971) 467.
5. D. G. CROWLEY, F. C. FRANK, M. R. MACKLEY and R. S. STEPHESON, *J. Polymer Sci. Polymer Phys. Ed.* **14** (1976) 1111.
6. R. J. GAYLORD, *ibid.* **14** (1976) 1827.
7. W. DIETRICH, G. REICHELT and H. TENKERT, *Chemiefasern/Text.-Ind.* **32** (1982) 612.
8. J. PETERMANN and R. M. GOHIL, *J. Mater. Sci.* **14** (1979) 2260.
9. J. PETERMANN, R. M. GOHIL and M. MASSUD, *ibid.* **17** (1982) 100.
10. R. M. GOHIL and J. PETERMANN, *J. Macromol. Sci. Phys.* **B18** (1980) 217.
11. J. PETERMANN and R. M. GOHIL, *J. Polymer. Sci. Polymer Lett. Ed.* **18** (1980) 781.
12. J. PETERMANN and H. GLEITER, *Phil. Mag.* **31** (1975) 929.
13. B. CAYROL and J. PETERMANN, *J. Macromol. Sci. Phys.* **B10** (1974) 305.
14. J. PETERMANN and J. GLEITER, *Phil. Mag.* **28** (1973) 1279.
15. V. P. CHACKO, W. W. ADAMS and E. L. THOMAS, *J. Mater. Sci.* **18** (1983) 1999.
16. A. W. AGAR, F. C. FRANK and A. KELLER, *Phil. Mag.* **4** (1959) 32.
17. R. HENDRICKS, *J. Appl. Crystallogr.* **11** (1978) 15.
18. W. A. RACHINGER, *J. Sci. Instrum.* **25** (1948) 254.
19. A. R. STOKES and A. J. C. WILSON, *Proc. Camb. Phil. Soc.* **40** (1944) 197.
20. I. G. VOIGT-MARTIN, *J. Polymer Sci. Polymer Phys. Ed.* **18** (1980) 1513.
21. G. R. STROBL, M. J. SCHNEIDER and I. G. VOIGT-MARTIN, *J. Polymer Sci. Polymer Phys. Ed.* **18** (1980) 1361.
22. I. G. VOIGT-MARTIN, L. MANDELKERN and E. W. FISCHER, *ibid.* **18** (1980) 2347.
23. I. G. VOIGT-MARTIN, L. MANDELKERN and E. W. FISCHER, *ibid.* **19** (1981) 1769.
24. W. W. ADAMS, D. C. YANG and E. L. THOMAS, in preparation.
25. R. HOSEMANN, *J. Polymer Sci.* **C20** (1967) 1.

*Received 30 June*
*and accepted 26 July 1983*